

**PROGRESS TOWARDS A COST-
EFFECTIVE ATOMIC FORCE
MICROSCOPE**

By

Jonathon Yuly

A thesis submitted in partial fulfillment of the
requirements for the degree of

Bachelor of Science

Houghton College

July 2016

Signature of Author.....
Department of Physics
July 12, 2016

.....
Dr. Brandon Hoffman
Associate Professor of Physics
Research Supervisor

.....
Dr. Kurt Aikens
Assistant Professor of Physics

**PROGRESS TOWARDS A
COST-EFFECTIVE ATOMIC
FORCE MICROSCOPE**

By

Jonathon Yuly

Submitted to the Department of Physics
on July 12, 2016 in partial fulfillment of the
requirement for the degree of
Bachelor of Science

Abstract

Work towards the design and construction of an atomic force microscope (AFM) is underway at Houghton College. In addition to yielding strong educational value, this device is intended to be used in the characterization of surface topography of thin metal films (such as Ag) and other solid state samples. Three separate “Johnny walker” designs have been designed and built, each design being informed by the previous ones. Though movement of any design has yet to be observed, the design and construction of an improved high voltage (~ 1 kV, 500 Hz) signal amplification system to drive the piezo-tube legs of the walker should improve the speed and reliability of future testing.

Thesis Supervisor: Dr. Brandon Hoffman
Title: Associate Professor of Physics

TABLE OF CONTENTS

Chapter 1	5
1.1 Overview	5
1.2 History	5
1.3 Motivation	10
1.4 Thin Metal Films	11
Chapter 2	16
2.1 Interatomic Potentials	16
2.2 Cantilevers as Harmonic Oscillators	17
2.3 Static Mode AFM	17
2.4 Tapping Mode AFM	18
Chapter 3	22
3.1 Overall Design	22
3.2 Isolation Mount	24
3.3 “Johnny Walker” Design	26
3.3.1 Mechanism.....	26
3.3.2 First Design.....	28
3.3.3 Second Design.....	30
3.3.4 Third Design.....	33
3.4 Control System	35
3.4.1 Overall Design.....	35
3.4.2 Cost-Effective Signal Amplifiers.....	37
Chapter 4	40
4.1 Progress	40
4.1.1 Signal Amplifiers.....	40
4.1.2 “Johnny Walker”.....	41
4.2 Future Plans	42
4.3 Conclusion	43

TABLE OF FIGURES

Figure 1. First published STM image.....	7
Figure 2. The first AFM design.....	8
Figure 3. An illustration of the optical beam deflection technique.....	9
Figure 4. An illustration of three cubic crystal structures.	12
Figure 5. An illustration of grain orientations and Miller indices.	13
Figure 6. STM images of an Ag thin film.....	15
Figure 7. An example of a Lennard-Jones potential.....	16
Figure 8. Illustration of the overall design.....	23
Figure 9. Eddy current dampening system.	25
Figure 10. An illustration of the walking mechanism.	27
Figure 11. A photograph of the walker ramp.....	28
Figure 12. The original Houghton walker design.	29
Figure 13. Schematic diagram of the second walker design.	31
Figure 14. Photograph of the second walker design.....	33
Figure 15. A photograph of the third walker design.....	34
Figure 16. Block diagram of the apparatus with control elements.....	36
Figure 17. A bipolar junction transistor (BJT) amplifier used to amplify signal V_{in}	37
Figure 18. A photograph of the walker control circuitry.	39
Figure 19. An oscilloscope trace of the response of the HV BJT linear amplifiers.	40
Figure 20. Three plots depicting the behavior of the HV transistor amplifier circuit.....	42

Chapter 1

INTRODUCTION

1.1 Overview

Microscopy, or the process of imaging structures that cannot be distinguished with the naked human eye, is essential to many fields of science, including the study of materials. Technological advancements in the science of microscopic imaging over the last several decades have been staggering, yielding many new forms of microscopy, including scanning force microscopy (SFM) and scanning tunneling microscopy (STM). Atomic force microscopy (AFM) is a special mode of SFM which has yielded images of non-conducting materials with resolution on the atomic scale [1].

1.2 History

Due to the discovery of important facts in modern physics, major advances in microscopy had already been made by 1980. One important innovation in the science of microscopy was the invention of the electron microscope in 1932, based on the improved understanding of electron beams [2]. Despite the fact that these new techniques had spatial resolution well above the optical diffraction limit, researchers were interested in still higher resolution. In 1982, G. Binnig and H. Rohrer had implemented a novel approach to microscopy, known as scanning tunneling microscopy (STM). This earned them the 1986 Nobel Prize in Physics [3], along with Ernst Ruska, who made fundamental contributions to electron optics, and invented the scanning electron microscope himself five decades earlier.

Scanning tunneling microscopy relies on quantum tunneling, a quantum mechanical phenomenon that allows particles to transverse a potential energy barrier whose energy maximum is higher than the kinetic energies of the particles striking the barrier (classically such a transversal is impossible). This

phenomenon is exploited by allowing electrons in a low voltage tip to tunnel onto a grounded conducting sample surface (the electrons tunnel because the tip does not actually have contact with the sample). In an ideal situation, the tunneling current is given by

$$J_T \propto e^{-Azs},$$

where $A = \sqrt{4m/\hbar}$, m being the electron mass and \hbar is the reduced Planck constant. In addition, z is the average thickness of the tunneling barrier, and s is the width of the barrier[4]. Because the tunneling current is exponential with respect to barrier height, a change in z of even a few angstroms can cause a change in the tunneling current by two or three orders of magnitude. This will happen when the tip is within a few nanometers from the sample. This allows the researcher to measure a surface topography to a high vertical resolution by transversely scanning the probe and changing the vertical position of the probe as needed to keep the tunnel current at some preset value [4].

Data from the first STM is shown in Figure 1. This data is a scan of the surface of a sample CaIrSn_4 . This material was chosen because Ir layers are chemically inert, so the scans could be conducted at rough vacuum ($\sim 10^{-6}$ Torr) [4]. The resolution capabilities of the STM are clear, as mono, double, and triple atomic steps are shown in both three dimensions and two.

One can see that the surface characterization capabilities of STM microscopy are impressive. However, this technology has a major shortcoming. In order for the electrons in the tip to tunnel through to the surface of the sample, and for the resultant current to be measured, the sample surface must be conducting. Of course, this is no issue if the samples to be examined are metals, and many samples can be made conductive by coating them with thin-metal films. However, some samples may be damaged by such coating. Also, it may be desirable to measure surface topographies *in-situ*, within some medium, such as water. Regardless, some surface detail will always be lost in the coating process.

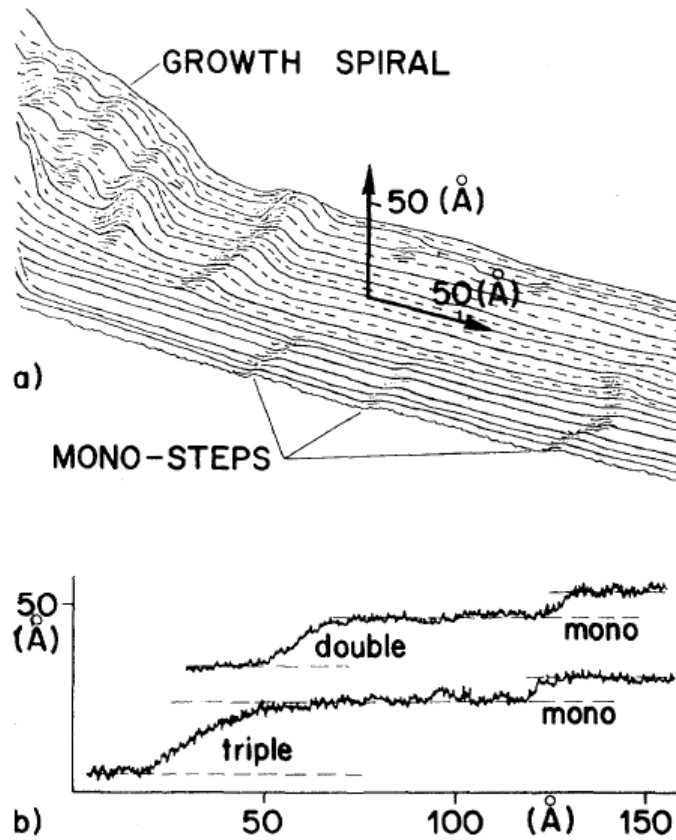


Figure 1. First published STM image. A CaIrSn₄ sample was scanned, producing results with clear mono, double, and triple atomic-sized steps. Figure taken from Ref. [4].

The atomic force microscope, which was originally designed to measure interatomic forces [1] is an answer to some of these problems. Binnig, Quate, and Gerber published [1] their work on this new technique in 1985. Binnig filed a US patent claim (US Pat. #4,724,318) [5] on the device in August of 1986. The basic design of the original AFM is shown in Figure 2.

The first AFM utilized the newly realized STM technology. A conducting lever with a sharp tip (parts 7 and 5 in Figure 2) was approached by a sample which could be moved in all of x-y-z by a piezo-electric crystal. The lever was deflected when the molecules in its tip began to interact with the molecules in the sample. This deflection was measured by the change in tunneling current across an STM probe, to

the conducting cantilever. This change in tunneling current was used as the source of a feedback signal to the piezo-crystal (3), which drove the sample towards or away from the tip on the cantilever, until the tunneling current returned to its predefined value (corresponding to a predefined cantilever deflection). The entire system was highly sensitive to vibrations, so Viton™ rubber pieces (24,17,19) and metal plates (23) were used to isolate the main AFM components from building vibrations.

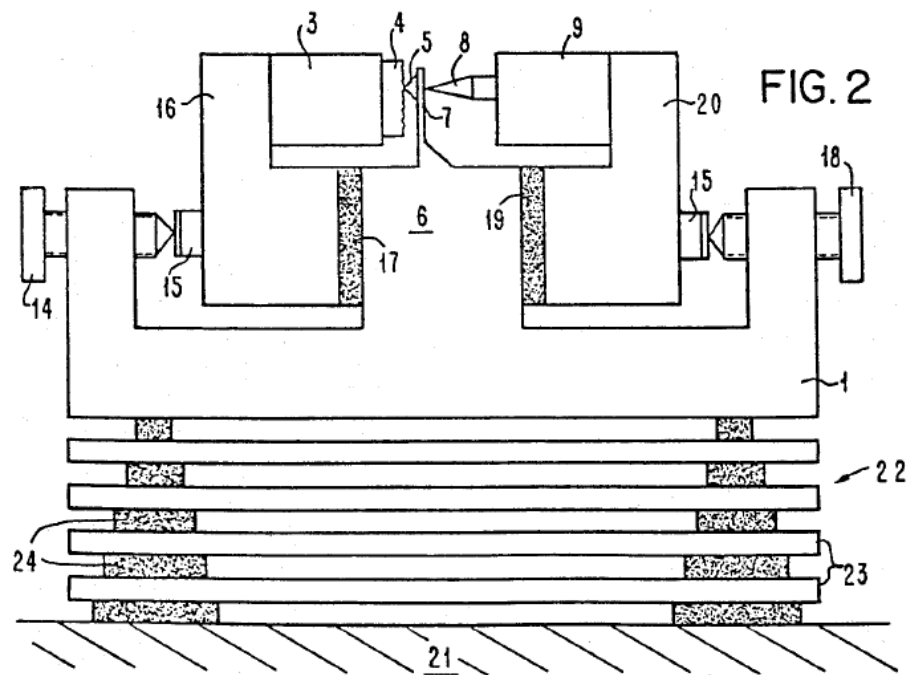


Figure 2. The first AFM design. A conducting lever (7) with small spring constant is attached to a sharp tip (5). This tip is approached by a sample (4) by means of a piezo-electric crystal (3) which moves the sample in all three dimensions during the scan. After the tip-sample distance is set, the scan begins. As the molecules in the tip interact with those in the sample, the cantilever beam is deflected, changing its distance from a STM tip (8). The tunnel current from (8) to (7) changes, and a feedback signal is sent to the crystal driving the sample movement (3) to pull the sample away from the probe tip, until the deflection of the cantilever returns to its pre-set value. Figure taken from Ref. [5].

As AFM technology developed and improved, new methods were developed to measure cantilever deflection. One major technique that is now used in many commercial and laboratory implementations of AFM technology is the optical beam deflection technique. Gerhard Meyer and Nabil Amer were the first to publish results using this technique [6]. This design has remained one of the most effective implementations of atomic force microscopy to date. However, other methods such as piezoresistive self-sensing cantilevers have been shown to be more sensitive under certain conditions [7]. The current design of the Houghton College AFM uses this technique, and progress towards an implementation of this technique has been made (See Chapter 3). The basic setup for this method is illustrated in Figure 3.

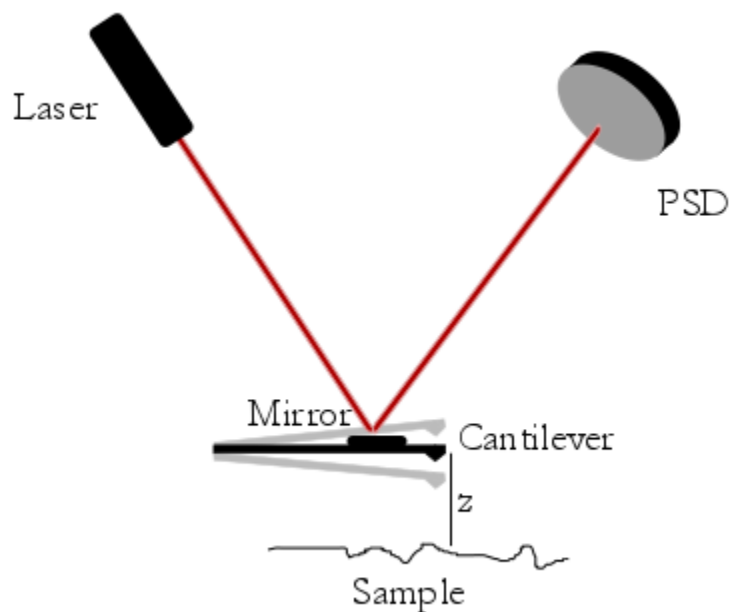


Figure 3. An illustration of the optical beam deflection technique. A laser is directed towards the cantilever, on which a small mirror is mounted. The laser reflects off this mirror into a position sensing diode (PSD). The cantilever is oscillated near its resonant frequency. As the cantilever stylus is scanned across the sample, the sample-tip distance, z , is kept constant by keeping the amplitude of the oscillations constant through a feedback circuit from the PSD to the device driving the cantilever oscillations.

This technique uses a laser and a position sensing diode (PSD) to measure the deflection of the AFM cantilever stylus. A laser is directed onto the cantilever, on which a small mirror is mounted. The cantilever is driven to oscillate close to its resonant frequency. The laser is reflected off of this mirror, into a PSD. This PSD can detect the small changes in the position of the laser-beam's footprint on its surface due to the cantilever's oscillations.

As the average tip-sample distance changes while the probe is being scanned across the sample, the amplitude of the cantilever's oscillations changes, due to forces between the cantilever tip and sample. The average distance between the tip and the sample can be held constant by changing the height of the cantilever such that the amplitude of the beam footprint's oscillation as detected by the PSD remains constant. This is often done using a feedback circuit.

1.3 Motivation

The primary motivation for the construction of an AFM device at Houghton College is its role in the study of thin metal films. Thin metal films are used in many applications, including microchips, mirrors, and data storage devices such as hard-drives. Therefore, understanding the properties of thin metal films, as well as how these properties change over time, under stress and various annealing temperatures, is important in characterizing and optimizing the lifetime of these devices. Impressive work has already been done in this area, using STM technology [8].

Houghton College has a laboratory devoted to thin-film studies and related research. An AFM device would be an excellent addition to this lab as part of its instrumentation, which currently includes a deposition chamber, a scanning electron microscope (SEM), a X-ray diffractometer (XRD), and an interferometer (the last two are anticipated to come on-line soon). An AFM device will complement the other instrumentation, allowing the laboratory to perform a wide variety of experiments in thin-film physics and related materials research.

Unfortunately, even low-cost commercial atomic force microscopes can cost as much as \$25,000 to \$50,000 [9]. To avoid this cost, a very low-cost AFM design must be drawn and constructed. This endeavor will also yield a great educational value.

The process of designing and constructing a cost-effective AFM for use in an educational setting seems possible. Remarkable progress towards this goal in an educational setting has already been made at Tsinghua University [10]. At Tsinghua University in 2013, researchers ranging from bachelor to PhD level worked to design and build a reproducible AFM device that could be deployed in high schools across China. They were challenged to implement a design costing less than \$1000. Even high school students were invited to participate, providing the teams with ideas concerning the future use of the new AFM devices. They were unable to reach their cost target. However, the educational value of this project was outstanding, and led to worldwide collaboration and the spawning of new centers in experimental education.

The technical motivation for the design and construction of the Houghton atomic force microscope is the study of thin metal films. Basic properties of thin metal films and as well as the intended use of the Houghton AFM are discussed next.

1.4 Thin Metal Films

A major motivation for an AFM at Houghton College is for the study of thin metal films, especially metals with a cubic crystalline structure. Many metals, including silver and copper, form a crystalline structure. A crystal is a state of matter which consists a lattice of atoms. This lattice is a repeating pattern in space that follows a translational symmetry which depends on the material. Many simple materials are cubic, such as silver, copper, and sodium chloride. A cubic crystal has a basic lattice structure with a cube shape. Two major types of cubic crystals are face-centered cubic and body centered cubic, as shown in Figure 4.

Bulk cubic crystal materials can be thought of as comprised of many cube shapes stacked on and beside each other, each cube sharing faces with its neighbor. In a primitive cubic (pc) structure, all of the atoms are located at the vertices of the cubes. In a body-centered cubic crystal, the atoms are located at the vertices of the cubes, and one at the precise center of each cube. In a face-centered cubic crystal, the atoms are located at each vertex, and also at the center of each face.

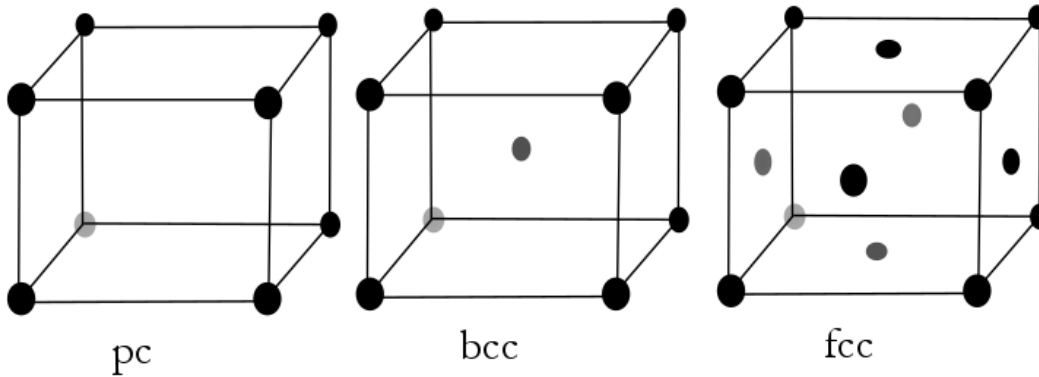


Figure 4. An illustration of three cubic crystal structures. The primitive cubic (pc) structure has each atom on a vertex of a cube. The body-centered cubic (bcc) structure has an atom on each vertex, and one in the precise center of the cube. The face-centered cubic structure holds one atom on each vertex, and one atom at the center of each face. This pattern repeats over and over again in the bulk material.

Cubic crystals are extremely common in research, and notation has been developed to unambiguously describe the orientation of grains within a bulk material. First, one can define some plane with respect to which the orientations will be described. In thin-film physics, this plane is often taken to be the plane of the substrate on which the crystalline film was deposited.

In order to characterize the orientation of some grain of cubic crystalline material with respect to the substrate, one can use the planes of atoms in the grain which are parallel with the substrate surface. Some vector that points orthogonal to these planes represents the orientation of the grain. This vector is notated using Miller index notation, as shown in Figure 5. For example, if some grain has a (100) orientation, one of the outer faces of the cubic cells is perpendicular to the substrate. If the grain has a (110) orientation, the plane defined by two diagonals of each cubic cell is perpendicular to the substrate. Planes of atoms defined by three vertices not on the same face are perpendicular to the substrate in (111) oriented grains. Note that the Miller indices can be written in any order, since the crystals have cubic symmetry.

Even among cubic crystals, the type of cubic structure and how that structure is oriented with respect to its neighboring grains has an impact on the properties of the bulk material. Grains are pieces of the polycrystalline material that all have the same orientation, and preserve the same symmetry throughout. Varying orientations of material inside a bulk crystal is an example of symmetry breaking, creating a clear grain boundary. Other types of symmetry breaking also exist such as twinning. Still other types of asymmetry exist which are not associated with grain differentiation, such as voids within a grain, or impurities embedded within a grain.

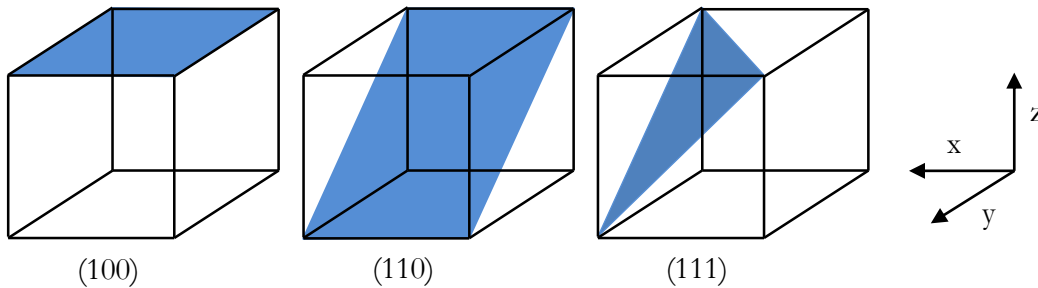


Figure 5. An illustration of grain orientations and Miller indices. Miller indices notate some vector that points orthogonally to planes of atoms within a grain that are parallel with some surface, often taken to be the substrate on which the crystalline material is deposited. If some grain has a (100) orientation, one of the outer faces of the cubic cells is perpendicular to the substrate. A (110) orientation describes a crystal in which the plane defined by two diagonals of each cubic cell is perpendicular to the substrate. If planes of atoms in a grain defined by three vertices not on the same face of each cubic cell are perpendicular to the substrate, the grain is (111) oriented. Because Miller indices describe cubic crystals, the components may be written in any order.

Often, grains will grow into larger grains, which allows the film to fall into a lower potential energy state. When two grains grow into each other, eliminating the gap between them, this further reduces the energy of the material, as two grain boundaries have more potential energy than one. Thus, grains will often grow larger during annealing, with annealing temperatures as low as room temperature and

colder. Sometimes, *much* larger (on the order of millimeters) grains grow to reach a much lower energy state. If the mechanisms behind the growth do not diminish with the size of the grains, this special process is called abnormal grain growth. In other words, the grains continue to grow even when this growth cannot be explained by the reduction in grain boundary surface area. The mechanisms behind abnormal grain growth are not completely understood, as accepted theoretical considerations have been shown to be inadequate in explaining some cases of it [11]. These topics are described here as examples of thin film phenomenology which can be studied using AFM microscopy.

Other researchers [7] have conducted experiments to measure the important initial stages of grain growth within a thin metal film using STM technology. Some of these results are displayed in Figure 6. The STM image (a) in Figure 6 displays a $175 \text{ nm} \times 175 \text{ nm}$ image of an Ag thin film (100 nm thick). The film was deposited at 270 K. Then, the film was annealed at 300 K for 15 hours, and another image (b) was taken. Much larger, faceted crystallites formed during the annealing. The orientation of these crystals was determined to be (111) and (100). This was inferred using the obvious 60° and 120° angles which the facets make at the edge of the crystals. (111) often forms 60° angles at interfaces, and (100) often forms 120° angles at interfaces. One of these interfaces is highlighted in Figure 6.

The Houghton AFM could be used to take similar images of Ag thin films, but these films do not have to be directly exposed in order to be conducting for STM imaging. An AFM could produce images of samples with oxide layers, protective films, or any other property which would prevent electrical conduction across them. This technique may allow additional insight into the nature of abnormal grain growth, continuing previous work done through Houghton College and Cornell University [11].

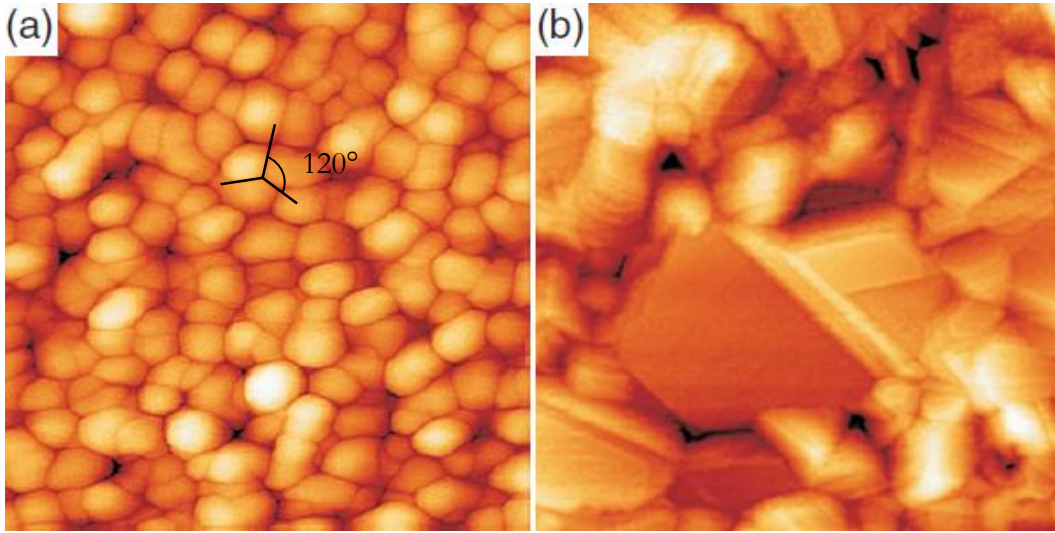


Figure 6. STM images of an Ag thin film (a) deposited to 100 nm of thickness at 270 K and then (a) annealed at 300 K for 15 hours. The orientation of the large, faceted (111) and (100) grains in (2) were inferred using the fact that their boundaries make frequent 60° and 120° angles. One such example of this is highlighted in (a). Each image is of size 175 nm × 175 nm. Figure taken from Ref. [8].

AFM topographical scans have also been found to be very effective for measuring sample surface roughness. If the relative height of the sample relative to the average height at point i is z_i and n points are measured, then the surface roughness is often characterized by the sum

$$R = \left(\sum_{i=1}^n \frac{z_i^2}{n} \right)^{1/2} . \quad (1)$$

Poon and Bhushan [12] found that AFM outperforms stylus profilometry and optical profilometry when measuring the surface roughness of glass-ceramic substrates (this material is used in making optical data storage disks, and measuring the surface roughness of these disks is important in quality control). The Houghton College AFM will likely be used in surface roughness characterization.

THEORY

2.1 Interatomic Potentials

Atomic force microscopy relies on interatomic forces to operate. The potential energy of interaction between any two atoms or molecules is often approximated using the Lennard-Jones potential [13], which is often of the form

$$U(z) = \epsilon \left[\left(\frac{z_\epsilon}{z} \right)^{12} - 2 \left(\frac{z_\epsilon}{z} \right)^6 \right], \quad (2)$$

where z is the distance between the atoms, ϵ is the minimum of the potential curve, and z_ϵ is the interatomic distance at which the interaction has potential $-\epsilon$. This potential curve is plotted in Figure 7. For a large distance z , the atoms or molecules experience a net attractive force. If the distance z is smaller than the equilibrium distance z_ϵ , then the interaction is repulsive.

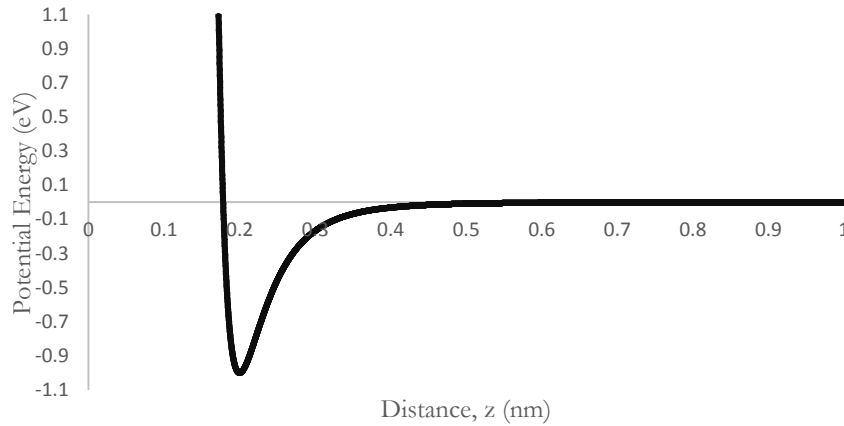


Figure 7. An example of a Lennard-Jones potential with $\epsilon = 1$ eV and $z_\epsilon = 0.2$ nm. If $z < 0.2$ nm, the interaction is repulsive, and if $z > 0.2$ nm, the interaction is attractive. There is equilibrium at $z = 0.2$ nm.

2.2 Cantilevers as Harmonic Oscillators

The cantilever of an AFM device can be modelled as a dampened spring with spring constant k and quality factor Q . When the tip approaches the sample to distance z , the atoms on the tip interact with those on the surface of the sample with a potential that is approximated as the Lennard-Jones Potential $V(z)$. Let z be the distance between the sample and the tip, z_0 be the equilibrium distance between the sample and the tip. The angular frequency of the cantilever's natural resonance can be written as $\omega_0 = \sqrt{k/m_c}$, where the effective mass of the cantilever oscillating in this mode is m_c , with effective spring constant k . Then the interaction between the sample and the tip acts as a driving or dampening force on the cantilever, and the system follows the equation of motion.

$$\frac{d^2z}{dt^2} = -\omega_0^2(z - z_0) + \frac{1}{m} \frac{dU(z)}{dz} - \frac{\omega_0}{Q} \frac{dz}{dt}. \quad (3)$$

The quality factor Q is given by $Q = 2\pi E/E_1$, where E is the total energy of the system, and E_1 is the energy dissipated from the system by frictional forces per oscillation cycle. Thus, if Q is large, then the amplitude of the cantilever's oscillation changes quickly, as energy quickly dissipates from the system. If Q is small (but the system is not over-damped), this process happens slowly.

This equation is very difficult to solve analytically. However, if the cantilever were held fixed, then $\frac{d^2z}{dt^2} = \frac{dz}{dt} = 0$. This greatly simplifies the process of extracting the potential function U from the deflection of the cantilever.

2.3 Static Mode AFM

In static mode, the cantilever does not vibrate. Instead, it is held still. This allows the experimentalist to measure the interaction force F_I directly, via a measurement of the cantilever's deflection as a function of the sample-tip distance:

$$F_I = -\frac{dU}{dz} = k(z - z_0) \quad (4)$$

This mode of operation is difficult to implement because the interaction potential has both an attractive and repulsive regime. Thus, unless the cantilever is very stiff, it will “jump to contact” with the sample across the potential minimum. If the cantilever is stiff, the deflections will be very small and difficult to measure.

2.4 Tapping Mode AFM

In order to probe the interaction potential without “sticking” to the sample, a dynamic mode of atomic force microscopy was devised. In this mode, the cantilever vibrates near its resonance frequency, and the inertia of its motion prevents it from sticking to the sample. In order to keep the cantilever in an oscillating state, a driving force is exerted on it (often using a piezoelectric ceramic). This changes the equation of motion (3) by adding a driving component to the force:

$$\frac{d^2 z}{dt^2} = -\omega_0^2(z - z_0) + \frac{1}{m} \frac{dU(z)}{dz} - \frac{\omega_0}{Q} \frac{dz}{dt} + A \cos \omega t. \quad (5)$$

The amplitude of this driving oscillation is A , and its frequency is ω . First, $U(z)$ can be written as its Maclaurin series around z_0 :

$$U(z) = U(z_0) + \left. \frac{dU}{dz} \right|_{z=z_0} (z - z_0) + \frac{1}{2} \left. \frac{d^2 U}{dz^2} \right|_{z=z_0} (z - z_0)^2 + \dots \quad (6)$$

Assuming that z does not vary much from z_0 , terms of higher order than two can be neglected in the approximation

$$U(z) \approx U(z_0) + c_1(z - z_0) + \frac{1}{2} c_2(z - z_0)^2, \quad (7)$$

where c_1 and c_2 are the first and second derivatives of U , respectively, evaluated at z_0 . Substituting this approximation of U into (5) gives

$$\frac{d^2z}{dt^2} = \left(-\omega_0^2 + \frac{c_2}{m}\right)z + \omega_0^2 z_0 + \frac{c_1}{m} - \frac{\omega_0}{Q} \frac{dz}{dt} + A \cos \omega t. \quad (8)$$

One can define a new variable

$$y = \left(-\omega_0^2 + \frac{c_2}{m}\right)z + \omega_0^2 z_0 + \frac{c_1}{m}. \quad (9)$$

Differentiation gives

$$\frac{dy}{dt} = \left(-\omega_0^2 + \frac{c_2}{m}\right) \frac{dz}{dt}. \quad (10)$$

Substituting these expressions into (8) yields

$$\frac{1}{\frac{c_2}{m} - \omega_0^2} \frac{d^2y}{dt^2} = y - \frac{\omega_0}{Q} \frac{1}{\frac{c_2}{m} - \omega_0^2} \frac{dy}{dt} + A \cos \omega t. \quad (11)$$

Rearranging

$$\frac{d^2y}{dt^2} = \left(\frac{c_2}{m} - \omega_0^2\right) (y + A \cos \omega t) - \frac{\omega_0}{Q} \frac{dy}{dt}. \quad (12)$$

To find a steady-state solution to this equation, assume a solution of the form $y = A_0 e^{i(\omega t + \delta)}$.

Substituting this expression into (12) yields

$$-A_0 \omega^2 e^{i(\omega t + \delta)} = \left(\frac{c_2}{m} - \omega_0^2\right) (A_0 e^{i(\omega t + \delta)} + A e^{i\omega t}) - i \frac{\omega_0 \omega}{Q} A_0. \quad (13)$$

Rearranging and using Euler's formula gives

$$\frac{-A_0 \left(\omega^2 + \frac{c_2}{m} - \omega_0^2 \right)}{A \left(\frac{c_2}{m} - \omega_0^2 \right)} = \cos \delta + i \sin \delta - \frac{i A_0 \omega_0 \omega}{A Q \left(\frac{c_2}{m} - \omega_0^2 \right)}. \quad (14)$$

This equation can be written as two separate equations, as the real and imaginary parts of the left and right sides must be equal:

$$\frac{-A_0 \left(\omega^2 + \frac{c_2}{m} - \omega_0^2 \right)}{A \left(\frac{c_2}{m} - \omega_0^2 \right)} = \cos \delta, \quad (15)$$

and

$$\frac{A_0 \omega_0 \omega}{A Q \left(\frac{c_2}{m} - \omega_0^2 \right)} = \sin \delta. \quad (16)$$

Squaring both equations and adding them together gives

$$\frac{A_0^2 \left(\omega^2 + \frac{c_2}{m} - \omega_0^2 \right)^2}{A^2 \left(\frac{c_2}{m} - \omega_0^2 \right)^2} + \frac{A_0^2 \omega_0^2 \omega^2}{A^2 Q^2 \left(\frac{c_2}{m} - \omega_0^2 \right)^2} = \sin^2 \delta + \cos^2 \delta = 1. \quad (17)$$

Solving for A_0 , the amplitude of the oscillation in y , gives

$$A_0 = \frac{A Q \left(\frac{c_2}{m} - \omega_0^2 \right)}{\sqrt{Q^2 \left(\omega^2 + \frac{c_2}{m} - \omega_0^2 \right)^2 + \omega_0^2 \omega^2}} \quad (18)$$

Thus, the amplitude of the oscillations in z is given by

$$A_z = \frac{A Q}{\sqrt{Q^2 \left(\omega^2 + \frac{c_2}{m} - \omega_0^2 \right)^2 + \omega_0^2 \omega^2}} \quad (19)$$

Since

$$c_2 = \left. \frac{d^2 U}{dz^2} \right|_{z=z_0} = c_2(z_0), \quad (20)$$

then the amplitude will change¹ as the average distance between the tip and the sample changes. This change is detected during a topographical scan, and the height of the sample relative to the cantilever is adjusted until the amplitude returns to some preset value. These adjustments are tracked and plotted, and the result is a topographical image.

It bears noting that when operating in dynamic mode, the value of the quality factor Q should not be large. A large Q value can make scanning images nearly impossible. As the tip scans across the sample surface, the average height of the tip relative to the sample will change. This will drive changes in the oscillation parameters of the cantilever. If Q is large, the cantilever will be slow in reaching a steady-state oscillation, and scan speeds will suffer as a result. If ten to hundreds of image pixels must be scanned every second, the cantilever must dissipate energy quickly enough to reach steady-state oscillations at least that many times per second. For more discussion on harmonic oscillators as applied to AFM technology, see [14]

¹ The phase δ of the oscillations can also change. This change can be tracked if desired.

Chapter 3

THE DESIGN

3.1 Overall Design

The basic outline of the Houghton College AFM design is depicted in Figure 8. Much of the recent progress towards the completion of this device concerns the “Johnny Walker” device (1,2,3,9 in Figure 8) and the optical deflection system (5,6,7). It bears noting that the design depicted in Figure 8 has not been fully assembled or tested to this date, as the individual components are still under construction. Progress concerning individual components has been made, and will be discussed in coming sections, as well as in the next chapter.

As seen in the figure, a circular plastic disk of radius 60 mm (1) will support a mount (2) on which samples will be placed, as well as three piezoelectric tube scanners (3). These tubes are attached with epoxy to this disk, and stand on small sapphire spheres (9), which are also attached to the tubes using epoxy. These tubes and their sapphire balls serve as legs of a Johnny walker, which will walk up and down a ramp (4). This walking movement is explained in section 3.3.

This walking movement will lower the sample towards a vibrating cantilever (5). A laser (6) reflects off of this cantilever and into a position sensing diode (PSD), a Conex PSD-9. The walker, cantilever, and ramp are supported by springs (8) attached to a supporting isolating mount (10). The springs, and an eddy-current dampening system (see Section 3.3) reduce building vibration to the vibration sensitive components.

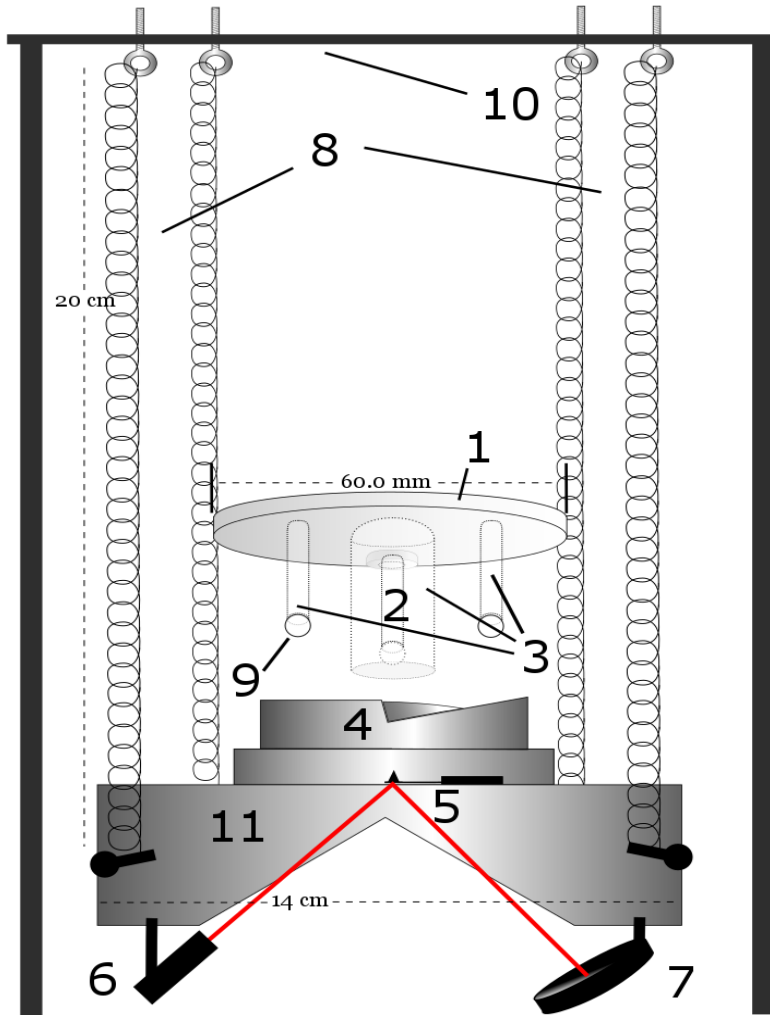


Figure 8. Illustration of the overall design of the Houghton College AFM. A circular plastic disk (1) will support the sample mount (2) and three piezoelectric tube scanners (3) which will stand on small sapphire spheres (9) acting as legs of a “Johnny walker”, which will walk up and down a ramp (4). This walking movement will lower the sample (on the sample mount (2)) towards a vibrating cantilever (5). A laser (6) reflects off of this cantilever and into a position sensing diode (PSD) (7). The walker, cantilever, and ramp are supported by a large circular base (11) which is suspended by springs (8) attached to a supporting structure (10).

3.2 Isolation Mount

We now discuss the mechanism of the isolation mount in more detail. When the large circular base (11) begins to vibrate with respect to the support structure (10), the springs will stretch or shrink a distance z from their equilibrium position z_0 . If the mass of the base and the apparatus is m_b , and the combined spring constant of the springs is the restoring force of the interaction is

$$F = -\frac{1}{2}k_s(z - z_0) - m_b g,$$

where g is the strength of the local gravitational field. One can define a constant $z'_0 = z_0 + \frac{m_b g}{k_s}$.

Substitution gives

$$F = -\frac{1}{2}k(z - z'_0).$$

This is the equation describing a linear restorative force with a new equilibrium, z'_0 . Thus, the springs serve the purpose of providing the system with a restorative force.

However, since this force only depends on the displacement from equilibrium, and not the speed of this motion, the system can resonate, losing energy to frictional dissipative processes alone. In fact, building vibrations can act as a driving force to the resonance. Thus, an eddy current dampening system will also be implemented to absorb vibrational energy from vibrational modes excited within the apparatus.

The eddy current dampening system is shown in Figure 9. When vibrations are introduced into the apparatus, the magnetic field at each point inside the large circular base will change. This is because the position of each point with respect to the magnet will be changing (the magnets are mounted to the outside frame, not the circular mount). By Faraday's Law, an electric field inside the large circular base will appear, given by

$$\nabla \times \mathbf{E} = \frac{\partial \mathbf{B}}{\partial t}$$

Since the circular base is a conductor, a current will immediately appear, counteracting the induced electric field. This current will absorb energy from the vibrations. This adds a restoring force on the base which is a function of its velocity, not position. Therefore, this isolation system exerts restorative forces to first and second order on the suspended apparatus.

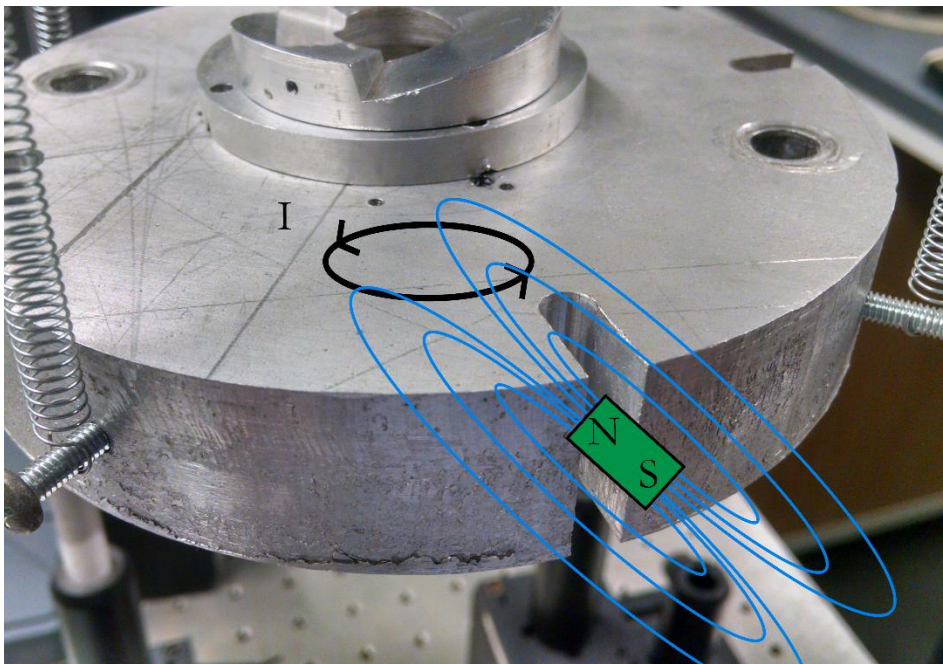


Figure 9. Eddy current dampening system. Magnets will be inserted into slots in the sides of the large conducting cylindrical base of the walker mount. When the mount begins to vibrate, the magnetic field inside the conductor will change, producing an EMF inside the mount. This EMF and the current I it generates will absorb the kinetic energy of the vibrations.

3.3 “Johnny Walker” Design

3.3.1 Mechanism

A “Johnny Walker” device is included in the Houghton AFM design. This device will provide coarse sample positioning as the sample approaches the cantilever. This device consists of three piezoelectric tube scanner “legs” with sapphire spheres epoxied to their bases (see Figure 8). This device “walks” up and down its ramp by taking small “steps” as illustrated in Figure 10.

The mechanism makes “steps” using a piezoelectric tube scanner. A sapphire sphere is attached to the base of the tube with epoxy. This acts a “leg” of the walker. Sapphire is smooth, so the coefficient of friction between the sapphire and the surface on which the walker is placed is minimal.

To begin the walking process, voltage is slowly applied across the tubes, causing them to bend (the second image in Figure 10). This voltage is applied slowly enough to prevent the sapphire from slipping across the surface. Then, the charge on the tubes is quickly discharged, causing the tubes to jump back into a straight position. This is done quickly enough to overcome the static friction between the sapphire and the surface, causing the leg to slip. After each iteration, the walker has shifted some distance (d in the figure) from its original position. Repeating this process can move the walker any desired distance. When properly placed with one leg on each ramp shown in Figure 11, the walker will shift up and down the ramps as this process is repeated.

The scanning tubes used in this walker device have five leads, four outer and one inner, as illustrated in Figure 11. The figure also illustrates the voltage configuration used during tube and walker tests. The inner lead and two outer leads are held at some constant voltage C (different depending on the tubes, voltage configuration, and desired tube deformation). The other outer leads, which stand opposite the leads held at a constant voltage, scan between 0 V and $2C$ in a saw tooth pattern. This voltage configuration creates a stronger average electric field throughout the volume of the piezoelectric ceramic than a configuration in which only one lead scans through the saw tooth pattern.

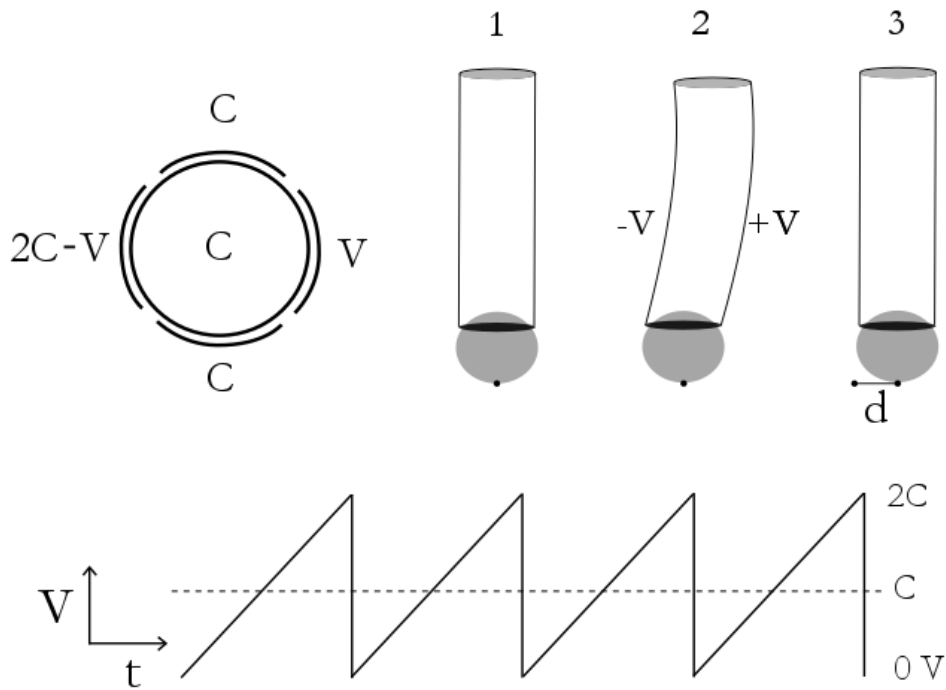


Figure 10. An illustration of the walking mechanism. Two outer leads and the inner lead of each piezoelectric tube scanner are set to some constant voltage C (different depending on the type of scanner). The scanners stand on small sapphire spheres which rest on a smooth surface (1). Each tube is slowly charged, changing V from 0 to $2C$, causing a relative voltage of $2V$ to appear across the tubes. This forces them to slowly bend (2). Then, the charge is very quickly removed from the tubes, forcing them to jump back to a straight position (3), overcoming the static friction between the sapphire sphere and the surface, shifting the tube over some distance d from its original position (the actual distance depends on many factors, especially the properties of the tube). This charge configuration across the tubes yields a stronger electric field in the tube than a configuration with a single scanning lead.

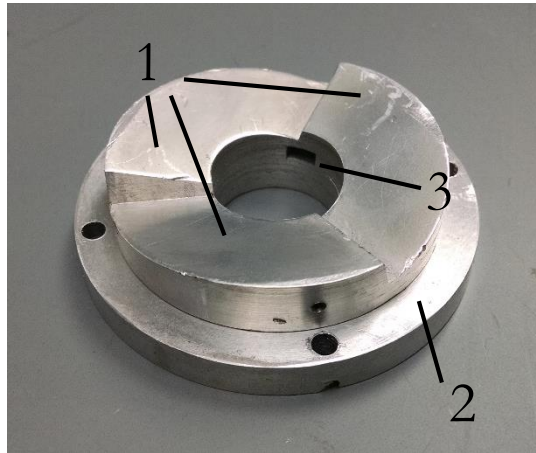


Figure 11. A photograph of the walker ramp. Three small ramps (1) were carved out of an aluminum disk, and a large hole was drilled through its center. These ramps are mounted on another aluminum disk (2) that is mounted on to the large circular ramp, (11) in Figure 8. In between these two disks, a small cavity (3) was carved, providing the space for the cantilever mount.

3.3.2 First Design

In 2009, a “Johnny Walker” was designed for the Houghton College AFM. This design was completed by Fall 2013. The final product is displayed in Figure 12.

This original design consisted of a thin aluminum disk on which three scanning tubes were attached using epoxy. Wires carrying charge to the tube leads (four outer leads and one inner lead per tube) were attached to their respective leads by layering a thin silver paste (16032 Pelco colloidal silver paste) over the wires, holding them fast to the leads. The wires were then fed through a cylindrical ceramic mounted to the top of the circular disk, leading them to the control circuitry.

This design exhibited several problems, causing it to be abandoned in favor of a second design. For instance, many components within this design were unnecessarily conducting. This caused many issues with electrical arcing.

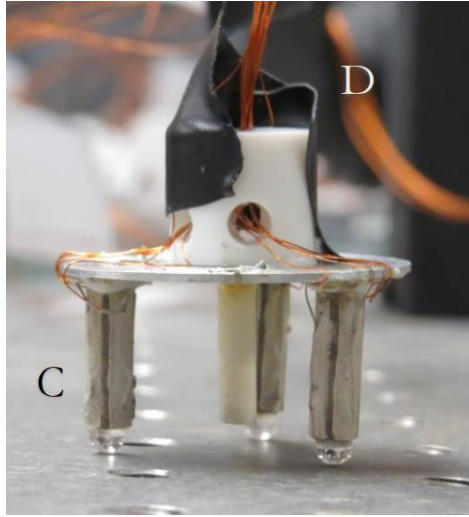


Figure 12. The original Houghton walker design. A circular aluminum disk was attached using epoxy to three piezoelectric tube scanners (C). Each tube scanner had five leads, four outer and one inner. A thin wire carried 0 – 1000 V to each outer lead. The inner leads were fed 500 V. These wires were pasted using a silver paste onto their leads, and fed through a cylindrical piece of ceramic with holes to the control circuit (D) Figure taken from Ref. [15].

The silver paste used to attach the wires to the tube leads exacerbated this problem, as the paste leaked between the leads. The tubes' outer leads were ≈ 1 mm apart, and they were to be charged to ≈ 1000 V. This is already near the dielectric breakdown of air at standard pressure and atmosphere, which has been measured to be as low as 2 kV at 1mm (hemisphere-hemisphere configuration) [16]. Thus, any paste leakage or cross-over can drastically reduce the stability of the circuit. Applying the silver paste uniformly and cleanly was exceedingly difficult.

Also, when this design was abandoned, it was believed that another design could be implemented which would allow easy access and maintenance of the scanning tubes. Removing or replacing the tubes in this first design was a tricky process. First, the epoxy holding the tubes to the disk must be carefully removed, keeping the tube itself undamaged. Next, the new tube must be carefully installed,

and new wires pasted to its leads, without disturbing any of the other tubes. Not only was this a time consuming process, but potentially harmful to the sensitive tubes.

The most concerning issue with this design was that, once each leg was assembled, it was impossible to verify that the wire carrying charge to the inner lead was making proper contact with the lead. This is because the only access to the inner leads is through the top or bottom of the tube. Once the leg is fully assembled, these access points are sealed off, by the circular disk at the top, and the sapphire sphere at the bottom.

3.3.3 Second Design

With these problems in mind, work towards a new walker design began in the Summer of 2014. This design was built the following term. The design is illustrated in Figure 13 and pictured in Figure 14.

Although similar to the previous design in many respects, several key improvements were added to this design. Firstly, every component that could possibly be insulating was rebuilt using a semi-transparent acrylic plastic. The radius of the circular disk was almost doubled in size, allowing easier handling and maintenance.

Three holes were drilled into this disk, each 20.0 mm from the center of the disk, and three plastic cylinders were attached to the disk centered over the three holes. These cylinders had larger holes drilled through their centers (in which the scanning tubes were inserted) and four smaller holes through the side of each cylinder, at $\approx 90^\circ$ angles with each other. These holes were tapped and screws were inserted into them. These screws served a dual purpose. They provided a light squeezing force to the tubes, holding them in place, while also conducting charge to the tubes' outer leads.

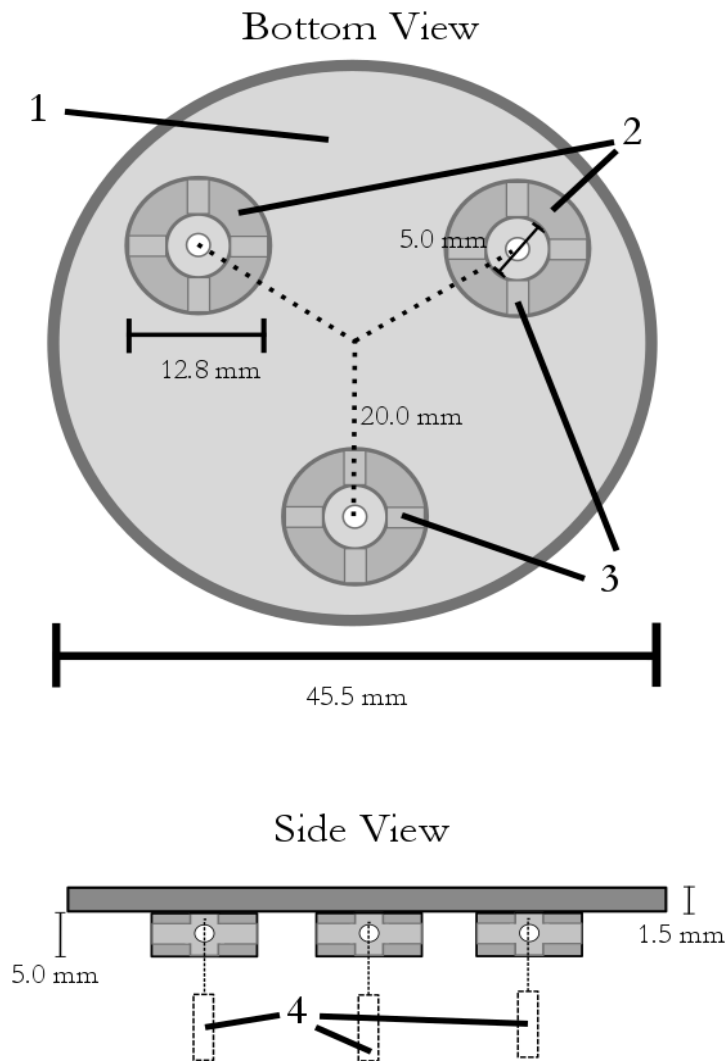


Figure 13. Schematic diagram of the second walker design. A thin disk of semi-transparent plastic (1) was cut and three small holes were drilled into it, each 20.0 mm away from the center of the disk. Using epoxy, three smaller circular disks of semi-transparent plastic (2) with larger holes (5 mm) through their centers were attached to the large disk as shown. Additional holes through the sides of the cylinders were drilled and tapped (3). Screws fed through these holes, holding the piezoelectric tubes in place. Thin copper wires fed 0-1000 V charge to the tube scanners' outer leads. Braided wire fed 500V volt charge to its inner leads through the small holes in the large circular disk (see Figure 14). The sample mount would be attached to the bottom of the large circular disk at its center.

Charge was carried to the screws by the same thin copper wire in the previous design, which was stripped of insulation at the end and wrapped around the screw to ensure contact. To properly charge the inner leads, thicker, braided wire was inserted through the small holes in the disk into the interior of the tubes. A photograph is shown in Figure 14.

This design had many advantages over its predecessor. Firstly, the semi-transparent plastic provided both electrical insulation and enhanced visibility. Electrical arcing in this design was greatly reduced, but when it did appear, the sparks were clearly visible through the plastic, so problems could easily be spotted.

Secondly, this system was greatly easier to maintain and handle. The screw-mounted tubes and the thin copper wires could be removed and replaced in a matter of seconds. Most of the electrical contacts could be easily tested, and at multiple locations. In addition, the apparatus could be almost entirely dismantled, leaving one component to be individually tested. All of these features were frequently used during testing. In fact, this flexible design was so reliable that it allowed problems both with the tubes themselves and the control circuitry to be revealed.

Lastly, due to the thick, braided wire that carried charge to the tubes' inner leads, it was more certain that proper electrical contact was being made with the inner leads. If the sapphire spheres were attached, access to the interior of the tubes was still impossible (this will always be the case). However, due to the bristly nature of the braided wire, proper electrical contact was more certain.

Unfortunately, it is believed that this walker design cannot be used in the final implementation of this device. During testing of this design and the control circuitry, it was determined that the on-site scanning tubes were cracked or otherwise no longer functioning properly. This was likely due to several factors. However, one possible source of unnecessary strain on the tubes was the mounting screws. To reduce strain on the tubes, they must be mounted vertically with minimal lateral pressure. Although not ideal, mounting the tubes with epoxy seems unavoidable.

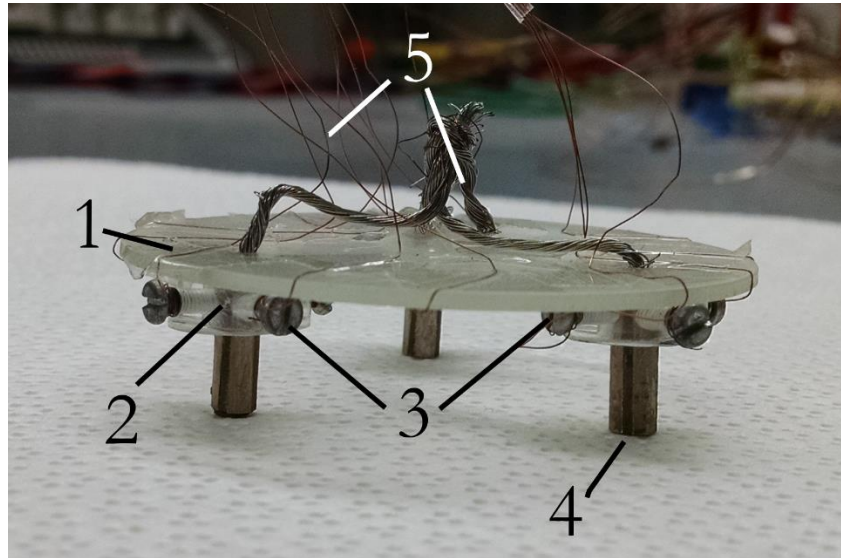


Figure 14. Photograph of the second walker design. A thin disk (1) of transparent plastic supports three plastic cylinders (2), in which the piezoelectric tube scanners were held in place with screws (3). Thin copper wires carry charge to the outer leads of the tubes (four per tube), while braided wire connected the inner lead of each tube to control circuitry.

3.3.4 Third Design

A third design, similar to the previous two but different in several important ways, was designed and implemented to eliminate or reduce problematic factors in previous designs. This design is photographed in Figure 15. A smaller circular mount (58 mm diameter, 2.8 mm thickness) was cut and three holes were drilled into it, each 15 mm from the center. New piezoelectric tubes (Boston Piezo Optics PZT-5H) with length 25.4 mm and outer diameter 3.91 mm, were epoxied over these holes. The holes had a diameter slightly less than that of the tubes. The leads were connected to the thin copper wires using a conductive epoxy (Epoxy International Silver-Bond 6 silver epoxy adhesive).

It is believed that this design improves upon the previous design mainly by reducing all unnecessary strain on the piezoelectric scanning tubes. The tubes are no longer mounted to the walker with screws,

but are instead attached with epoxy. Wires are also attached to the tube leads using a silver based conducting epoxy. This eliminates as much strain as possible on the tubes. In order to promote access the inner leads, the holes over which the tubes were mounted are larger than the holes in the previous design. They are large enough for a small probe to be inserted into the center of the tubes if necessary to test for proper electrical connection of the inner leads.

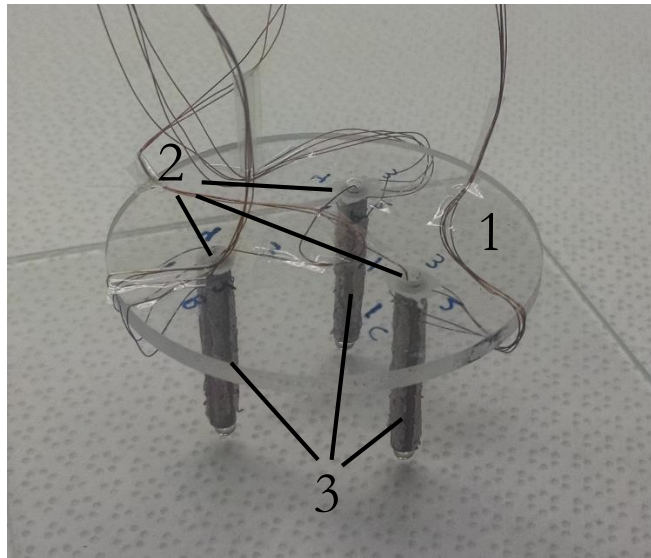


Figure 15. A photograph of the third walker design. A slightly smaller acrylic disk (1) was cut and three holes (2) slightly smaller than the diameter of the scanners were drilled into this disk forming an equilateral triangle centered at the center of the disk. Three new piezoelectric tube scanners were epoxied over these holes. Wires were epoxied to the scanner leads (including the inner leads) using a conductive silver epoxy.

This design is currently undergoing testing. It is too early in this process to conclude whether or not this design will be successful or not. Movement of the walker has yet to be observed.

3.4 Control System

3.4.1 Overall Design

In order to control and obtain data from the Houghton AFM device, a control system similar to that illustrated in Figure 16 must be designed and implemented.

The laser beam will be reflected off a vibrating cantilever which will be interacting with a sample. The footprint of the laser beam will be measured on the surface of a position sensing diode PSD (Conex PSD-9). The oscillation parameters of the motion will be read into a comparator, which may perhaps be implemented as software. This comparator will compare the oscillation parameters of the beam footprint with those of the driving signal to the cantilever's motion. When these oscillation parameters change, this will indicate that the distance between the cantilever tip and the sample surface has changed.

The output of the comparator will be read into a computer. The computer will decide if the height of the sample needs to change, in order to keep the cantilever at some fixed distance from the sample surface, and thus keeping the cantilever oscillation frequency constant. If necessary, the computer will produce a new command which will be sent to a waveform generator, which generates the signal required to walk, or a constant offset to finely adjust the sample position.

The waveform generator will produce two types of signals, one which is intended to drive the cantilever motion, and the other which is intended to control the tube scanners on the Johnny walker. These signals will be amplified using a bipolar junction transistor (BJT) amplifier described in the next section. Together these signals will complete the feedback system, allowing this AFM device to automatically adjust the sample position, holding the cantilever oscillation frequency constant as the tip is scanned across the sample.

The voltage difference between the inner leads of the piezo tubes and the outer leads determines the height of the walker, as the lengths of the tubes change slightly when this voltage difference changes. To produce an image, the voltage to the inner leads of the piezo tubes will be tracked, and plotted

against the voltage to the outer leads, which determines the x-y position of the walker. This will yield an image representative of the topography of the sample. Of course, to measure the actual distances between topographical features, this method must be calibrated to a sample of known topography.

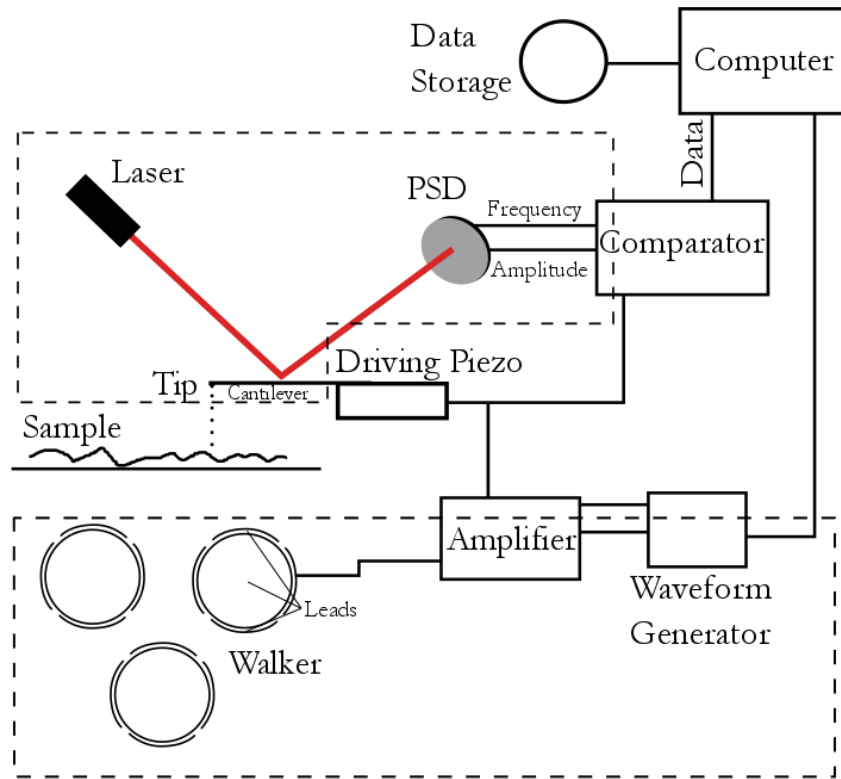


Figure 16. Block diagram of the apparatus with control elements. The sections enclosed in the dashed line are currently undergoing construction and/or testing. The vibration parameters of the laser footprint on the PSD (Conex PSD-9) are read into a comparator (perhaps in software), which compares the oscillation parameters of the driving signal of the cantilever with those of the beam footprint. The computer can save this information as image data, and send instructions to a waveform generator which creates signals that are amplified, driving the piezoelectric ceramics in the walker and mounted to the cantilever, completing a feedback system.

3.4.2 Cost-Effective Signal Amplifiers

In order to reduce the cost of the Houghton College AFM design, a system of bipolar junction transistor (BJT) amplifiers were implemented to provide the driving signal to the piezoelectric components driving the cantilever and the walker device. The basic design of a BJT transistor amplifier is illustrated in Figure 17.

To amplify a signal V_{in} , it is directed through a small resistor ($R \approx 220 \Omega$) to the base lead of a high-voltage npn transistor (International Rectifier IRG4PH40UDPbF). The emitter lead is connected to ground. The collector lead is connected through a large resistor ($R' \approx 10 M\Omega$) to the high-voltage source, an EMCO C20 regulated high voltage power supply. The amplified signal V_{out} was found to be over three orders of magnitude greater than the input signal. This is described in more detail in the next chapter.

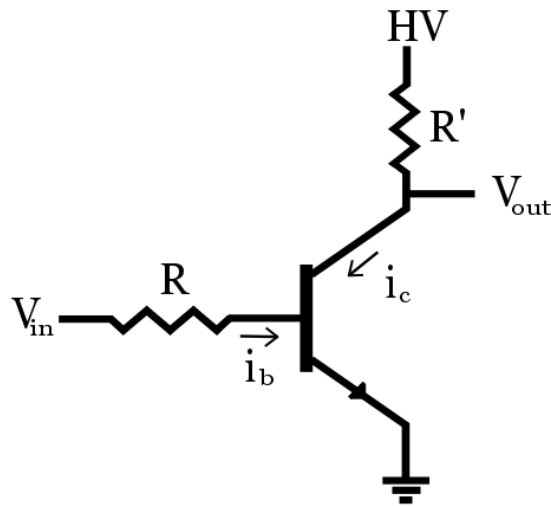


Figure 17. A bipolar junction transistor (BJT) amplifier used to amplify signal V_{in} . In the active region of an npn transistor, the current through the transistor is given by $i_b \propto i_c$. For use in the Houghton AFM design, high voltage npn transistors were used. The amplified signal V_{out} is over three orders of magnitude greater than the input signal.

In the active region of an npn BJT, the collector current i_c is proportional to the base current i_b . Thus, if a signal V_{in} is applied across the transistor at its base, then this signal will be inverted and amplified at V_{out} . The actual behavior of the transistor amplifiers used is characterized in the Results section.

The control circuitry for the walker device is pictured in Figure 18. As seen in the photograph, multiple EMCO amplifiers were used. Each amplifier powered a separate BJT amplifier. This was done because the EMCO amplifiers can only output ≈ 0.5 mA of current. Thus, it was thought that only one amplifier would not be able to power the entire walker and the control circuitry, without at least occasional overloading during an operational cycle.

The control circuit in Figure 18 has currently been wired to create only two signals for testing. To the right, a voltage divider system was designed to linearly scale down the higher voltages to be more manageable for measurement.

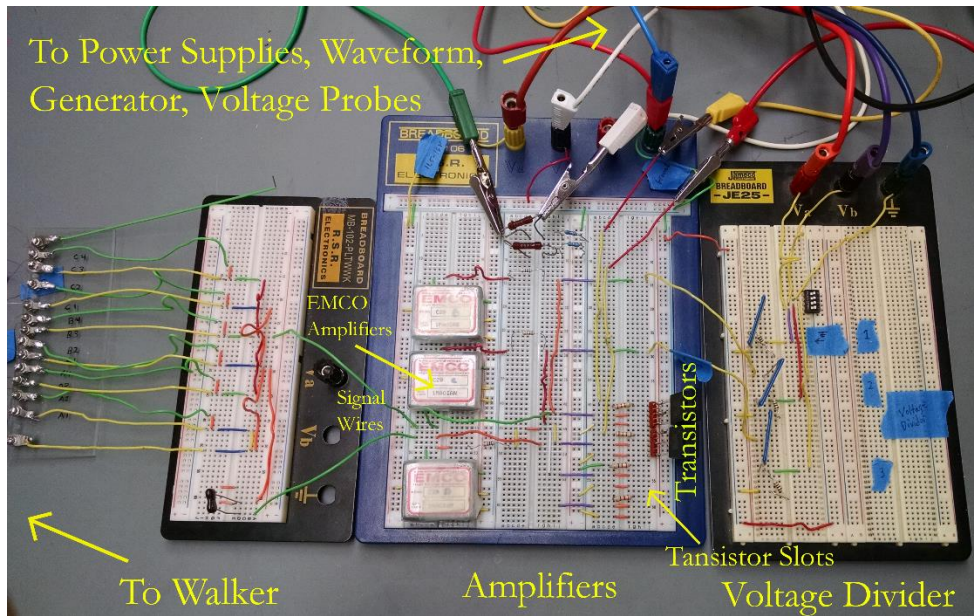


Figure 18. A photograph of the walker control circuitry. Here the circuit is wired to perform a basic test of the walker device. Only two signals are produced by this circuit: one for two outer leads of the tube scanners, and one for the other two outer and the inner leads. To the right, a voltage divider system was constructed to measure the high voltage signals at a more manageable voltage. Multiple EMCO amplifiers were used to prevent any current draw from the transistors and the walker from overloading any one EMCO amplifier.

Chapter 4

PROGRESS, FUTURE PLANS, AND CONCLUSION

4.1 Progress

4.1.1 Signal Amplifiers

The control circuitry for the walker device is working as expected. A saw tooth waveform can be produced at voltages as high as 1000 V and higher and speeds of ~ 500 hz. Figure 19 shows an oscilloscope trace of the output of the HV amplifiers.

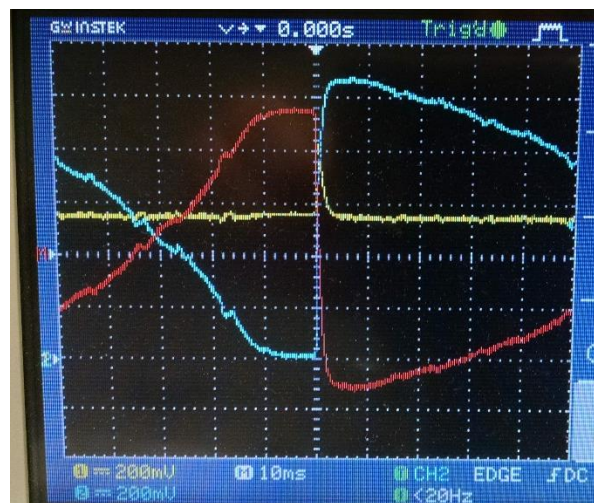


Figure 19. An oscilloscope trace of the response of the HV BJT linear amplifiers. The Blue trace is the output of one of the BJT amplifiers with a saw tooth input (this signal is inverted), and the yellow trace is the output of another BJT amplifier with a constant voltage applied to its base. The red trace is the difference between them. The voltage has been scaled down to the oscilloscope. Each volt in the trace scales to ≈ 500 V in amplifier output. The circuit has some capacitance, yielding a time constant of ≈ 3 ms.

The blue trace is the output of one of the HV BJT amplifiers with a saw tooth waveform applied to its base. The yellow trace is the output of another BJT with a constant voltage applied to its base. The red trace is the difference between them. The range of voltages is ≈ 1 V over this trace, but this voltage is being measured at the base of a voltage ladder. One volt in Figure 19 corresponds to ≈ 550 V of amplifier output. The circuit has some capacitance (originating in the EMCO amplifiers themselves) corresponding to the ≈ 3 ms time constant observable when the saw tooth input goes high. Applying this signal to the piezo tubes did not significantly alter the decay constant of the circuit.

The active region of the HV transistors was found to be approximately in the range $3.70\text{ V} \leq V_{in} \leq 3.95\text{ V}$, when $V_{out} \approx 1000\text{ V}$ and $R \approx 10\text{ M}\Omega$. Figure 20 displays the output voltage of the BJT amplifiers over a range of input voltages.

Three plots in Figure 20 show the range of BJT amplifier output for (a) $R = 40\text{ M}\Omega$, (b) $R = 10\text{ M}\Omega$, and (c) $R = 1\text{ M}\Omega$. The constant line above the output curves is the output of an EMCO amplifier without a BJT amplifier. The HV BJTs must continually draw some current ($\sim 10\text{ }\mu\text{A}$), even while inactive. This explains the offset voltage when the BJT is applied, as the BJT itself is applying a load to the EMCO output.

The new piezoelectric scanner tubes (Boston Piezo Optics PZT-5H) have lower operating voltages ($\approx 120\text{ V}$) than the previous tubes. It has been observed that the response of the EMCO amplifiers and the BJTs is different in this lower voltage regime. The behavior of the circuit at lower voltages needs to be better characterized and understood and any necessary adjustments need to be made, before serious testing of the walker device under these new conditions can be performed.

4.1.2 “Johnny Walker”

Two initial “Johnny walker” designs were discarded due to various performance and other issues (See Sections 3.3.2 and 3.3.3). Construction and testing of the third walker design (Section 3.3.4) remains underway as of May 2016. No movement has yet been observed with this design. This final design

may yet be shown effective, but the lower voltage amplifier signal to the new piezo actuators must be verified before a rigorous test of the new design can be carried out (see Section 4.1.1).

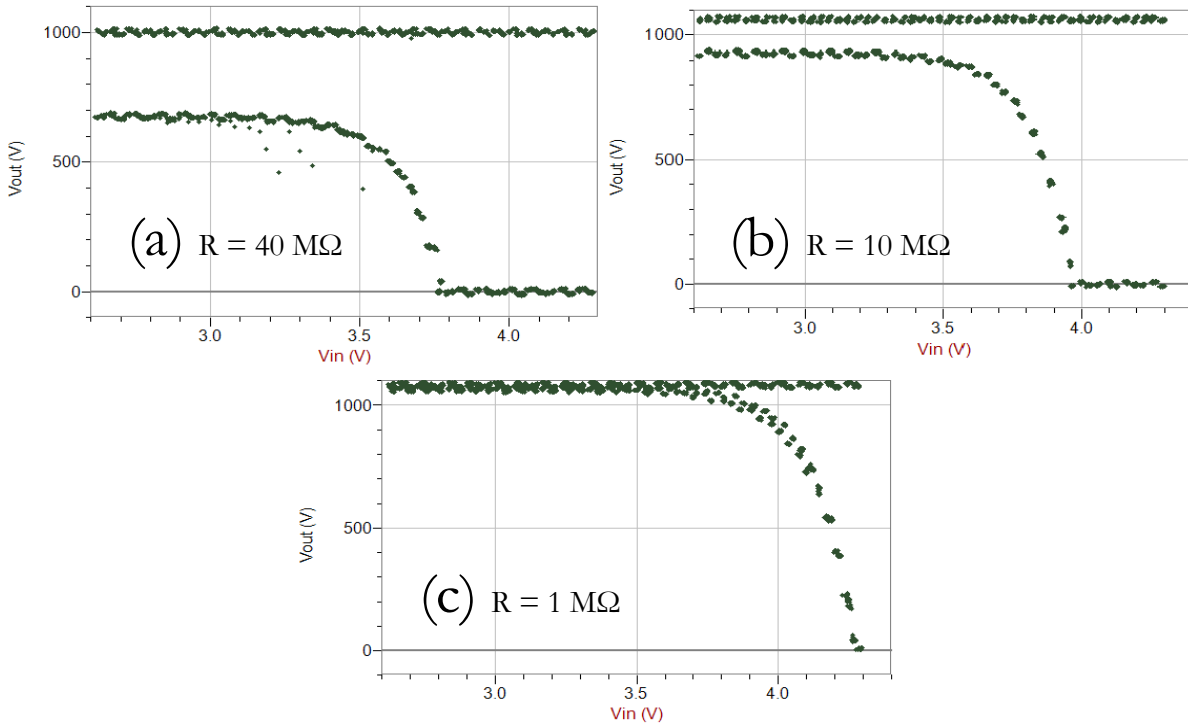


Figure 20. Three plots depicting the behavior of the HV transistor amplifier circuit with different values for R (see Figure 17). The output when $R = 40 \text{ M}\Omega$ is plotted in (a). In (b), the output is plotted for $R = 10 \text{ M}\Omega$. In (c), a plot showing the range of output voltages when $R = 1 \text{ M}\Omega$ is shown. The constant line above the curves is the output of the EMCO amplifiers without the BJTs. The increasing offset with R indicates a slight current through the BJTs even when inactive.

4.2 Future Plans

Assuming the signal to the piezo legs will be properly verified and adjusted as needed, several steps must be performed before the walker device can be completed. Firstly, when movement of the walker is seen, it must be reproduced and characterized to ensure that slippage of the device only occurs at desired times, and that all of the legs are moving uniformly and consistently. This could be done by

changing the speed of the walking signal, to check that the speed of the walking motion is proportional to the signal frequency.

After the walker device is reproducibly functional, the optical detection system must be implemented. This will require focusing a laser beam onto a small cantilever, and reflecting that beam into a position sensing diode (PSD). Once this is complete, the cantilever must be driven to oscillate, and the oscillation of the beam footprint on the PSD must be observed. Progress has been made towards this end, as a beam has been successfully reflected off of a cantilever. This progress will be described in an upcoming undergraduate thesis [16].

Both of these major steps must be taken before work towards obtaining images can begin.

4.3 Conclusion

Some progress towards the design and construction of an atomic force microscope has been made at Houghton College. Several “Johnny walker” designs have been designed and implemented, each building off the success and failure of its predecessors. Also, an isolation mount and walker ramp have been machined and assembled. Lastly, control circuitry which can generate HV signals to the walker’s piezo legs has been designed and implemented. This circuit can generate signals as high as 1000 volts and higher at speeds of 500 hz.

Once the major steps outlined in Section 4.2 are completed, work towards obtaining topographical images can begin. This AFM is intended to be used in the characterization thin metal films on site at one of the research laboratories at Houghton College. It is hoped that the continued work towards the implementation of this technology and its use afterwards will continue to be an excellent educational venture.

References

- [1] G. Binnig, C.F. Quate, and C. Gerber, Phys. Rev. Lett. **56**, 9 (1986).
- [2] Ruska, E., and M. Knoll, Z. Techn. Physik **12**, (1931).
- [3] Press Release: The 1986 Nobel Prize in Physics. Royal Swedish Academy of Sciences, (1986).
- [4] G. Binnig, H. Rohrer, C. Gerber, and E. Weibel, Phys. Rev. Lett. **49**, 1 (1982)
- [5] G. Binnig, *U.S. Patent No. 4,724,318*. Washington, DC: U.S. Patent and Trademark Office, (1988).
- [6] G. Meyer and N. M. Amer, Appl. Phys. Lett. **53**, 24 (1988).
- [7] M. Dukic, J. Adams, G. Fantner, Scientific Reports, **5**. (2015).
- [8] C. Polop, C. Rosiepen, S. Bleikamp, R. Drese, J. Mayer, A. Dimyati, T. Michely, New Journal of Physics **9**, 74 (2007).
- [9] AFM Workshop price listing, WWW Document, <http://www.afmworkshop.com/atomic-force-microscope-prices.html>. (Accessed 5/27/2016).
- [10] F. Grey, Nature Nanotech. **10**, 480 (2015).
- [11] S. P. Baker, B. Hoffman, L. Timian, A. Silvernail, E. A. Ellis, Acta Materiala **61**, 19 (2013).
- [12] C. Poon, B. Bhushan, Wear, **190**, 1 (1995).
- [13] J. Lennard-Jones, Proc. Phys. Soc., **43**, 5 (1931).
- [14] B. Bhushan, *Applied Scanning Probe Methods*. (Springer-Verlag, Berlin, 2004), Vol. 2, Ch. 1.
- [15] E. Ocock, B.S. thesis, Houghton College (2013).
- [16] P. Singh, S. Kumar, S. Sinha, Res. J. Engineering Sci., **2**, 12 (2013).
- [17] H. Kroening, B.S. thesis, Houghton College (2016).